Suppressing Förster Resonance Energy Transfer Between Organic Dyes on a Co-Sensitized Metal-Oxide Surface

Viktoras Dryza* and Evan J. Bieske

School of Chemistry, The University of Melbourne, Victoria, Australia 3010

E-mail: vdryza@unimelb.edu.au

Phone: +613 8344 8163. Fax: +613 9347 5180

*To whom correspondence should be addressed

Abstract

Time-resolved fluorescence spectroscopy is used to investigate the efficiency of Förster resonance energy transfer (FRET) between two different types of organic dye sensitizers bound to zirconia nanoparticles. The co-sensitization scheme involves using the IR125 dye as the FRET acceptor and either the D149 dye or D35 dye as the FRET donor, with the FRET parameters determined by monitoring the donor dye's excited state lifetime in the absence and presence of the acceptor dye. The FRET rate is found to be faster for the D149+IR125 pair than for the D35+IR125 pair. From the FRET quantum yields, the Förster distances for the D149+IR125 and D35+IR125 pairs are estimated to be 3.5 and 2.6 nm, respectively. Analysis of the data, in conjunction with time-dependent density functional theory calculations, leads to the conclusion that the variation in the Förster distances is dictated mainly by differences in the donor-acceptor orientation factors. For D149 the rhodanine acetic acid binding group constrains the dye to lie almost parallel to the surface, whereas the cyanoacrylic acid binding group of D35 causes the dye to sit almost perpendicular to the surface. Because IR125 lies parallel to the surface, due to the two sulfonate binding groups, there is better alignment of the transition dipole moments for the D149+IR125 pair than for the D35+IR125 pair. Deliberately choosing dyes with binding motifs that misalign the donor-acceptor transition dipole moments may be an effective strategy for suppressing FRET within dye-sensitized solar cells to enhance their efficiency.

1 Introduction

Dye-sensitized solar cells (DSSCs) are promising candidates as next-generation solar cells.[1–4] The main benefits of DSSCs are that they work well in diffuse sunlight and can be constructed using cheap, environmentally friendly materials. A DSSC's response to solar radiation is largely dictated by the absorption spectrum of the molecular dye anchored to a titania anode electrode, together with the efficiency with which the excited dye molecules

inject electrons into the circuit. Ideally, the dye should absorb light strongly across the entire visible and near-IR regions. However, in practise no single dye satisfactorily performs this task. This is especially pertinent for organic dyes, which have the advantages of high absorption coefficients and being composed of abundant elements, but typically absorb light over a narrower range than ruthenium-based organometallic dyes.[5] To engineer panchromatic DSSCs, co-sensitization with two dyes having complementary absorption spectra has been employed,[6–15] with a DSSC based on this approach achieving one of the best recorded DSSC conversion efficiencies.[16]

Although co-sensitization is an effective strategy to broaden a DSSC's spectral response, achieving better performance than a mono-sensitized device is not straightforward. Problems can arise because the dyes have different uptake rates during the sensitization process, due to their different mobilities through the porous electrode and surface binding affinities.[8] Furthermore, intermolecular interactions between the two dyes can occur, including Förster resonance energy transfer (FRET) from the excited, short-wavelength dye to the long-wavelength dye.[6,7,10,11,14] FRET is usually detrimental because the electron injection efficiencies of the best near-IR organic dye sensitizers are currently lower than those of the best visible organic dye sensitizers.[2,3,6,7] In addition, the IR dye can degrade more rapidly as it performs more of the electron injection.[6] FRET between different dyes can be prevented by constructing multi-layered metal-oxide electrodes, with the dyes confined in different layers.[17,18] Alternatively, FRET can be embraced in schemes where only the acceptor dye is attached to the electrode, with the donor dye either doped in the electrolyte or tethered to the acceptor dye using a molecular chain.[19–25]

In this study, we use time-resolved fluorescence spectroscopy to investigate whether FRET between two different organic dyes on co-sensitized metal-oxide nanoparticles (NPs) can be suppressed by deliberately misaligning the transition dipole moments of the donor and acceptor dyes. This is achieved by selecting dyes possessing different surface-binding groups, which govern the relative orientation of the two dyes on the surface. This

approach potentially maximises the light-harvesting efficiency of a co-sensitized DSSC by insulating the donor dye's excited state against FRET, preserving its superior electron injection capacity (relative to the acceptor dye).

2 Experimental and computational approach

A detailed description of the experimental and computational approach is given in S1. Briefly, D149 and D35 donor dye solutions (0.1 mM, acetonitrile:tert-butanol, 1:1), a IR125 acceptor dye solution (0.1 mM, methanol), and a chenodeoxycholic acid (CDCA) co-adsorbent solution (2 mM, acetonitrile:tert-butanol, 1:1) were used to make sensitizing solutions that were reacted with zirconia NPs. Sensitizing solutions were prepared with either only a donor dye, or both donor and acceptor dyes, with all solutions having a CDCA:donor dye ratio of 50:1. Abbreviated descriptions of the samples are given by the dye(s) attached, the metal-oxide NP (zirconia = Zr), and the donor:acceptor dye ratio within the sensitizing solution (C1 = 18:1, C2 = 9:1).

To collect the fluorescence spectra of the dye-sensitized NPs, the samples were supported on a glass slide and held inside a vacuum chamber containing 1 Torr of nitrogen buffer gas. The attached dye molecules were excited with laser pulses ($\sim$12 ps, $\sim$5 mW/cm^2, 82 MHz) from a 532 nm diode-pumped Nd:YAG laser. For the dispersed emission experiments, the collected fluorescence was passed through a 532 nm long-pass filter, and sent to a spectrometer equipped with a charge-coupled device detector. For the time-correlated single photon counting (TCSPC) experiments, the collected fluorescence was passed through a 635–675 nm band-pass filter, transmitting only fluorescence originating from the donor dye, and sent to a cooled photomultiplier tube connected to a TCSPC card.

The properties of the D149, D35, and IR125 dyes were explored theoretically using density functional theory [CAM-B3LYP/6-31+G(d)] within the Gaussian 09 program.[26,27]

The lowest energy isomers of the gas-phase dyes were located and subject to a vibrational frequency analysis, with their excited electronic states examined using time-dependent density functional theory (TD-DFT).

3 Results and discussion

3.1 Spectroscopy of the organic dyes in solution

Two commercially available DSSC organic dye sensitizers (D149, D35) were used in this study,[28,29] together with a near-IR organic dye (IR125) that functions as a DSSC sensitizer.[30] The molecular structures of the dyes are shown in Figure 1. These dyes are ideal for light-harvesting because they possess strong electronic charge-transfer absorptions, where the excited electron is promoted from an electron donor motif to an electron acceptor motif, with the latter also incorporating an acidic group that binds the dye to the metal-oxide surface. The electron donor motifs for D149, D35, and IR125 are indoline, triphenylamine, and heptamethine, respectively, whereas the electron acceptor/binding motifs are rhodanine acetic acid, cyanoacrylic acid, and benzoindolium butane-1-sulfonate, respectively.

The absorption and emission spectra of the three dyes in solution are shown in Figure 2. D149 and D35 display broad $S_1 \leftarrow S_0$ absorption bands with maxima at 530 and 480 nm, respectively. The D149 and D35 emission bands have maxima at 640 and 625 nm, respectively. The $S_1 \leftarrow S_0$ absorption band of IR125 is much narrower than that of D149 and D35 and has a maximum at 785 nm. Furthermore, its Stokes shift is small, with its emission band maximum located at 830 nm. This indicates that the ground and excited state geometries are similar for IR125, but are quite different for D149 and D35, most likely due to the greater charge-transfer character of the latter dyes' absorptions.

FRET involves non-radiative electronic energy transfer between two chromophores via long-range dipole-dipole coupling.[31,32] For efficient FRET between donor and acceptor dyes, certain criteria must be met: good spectral overlap between the donor's emission

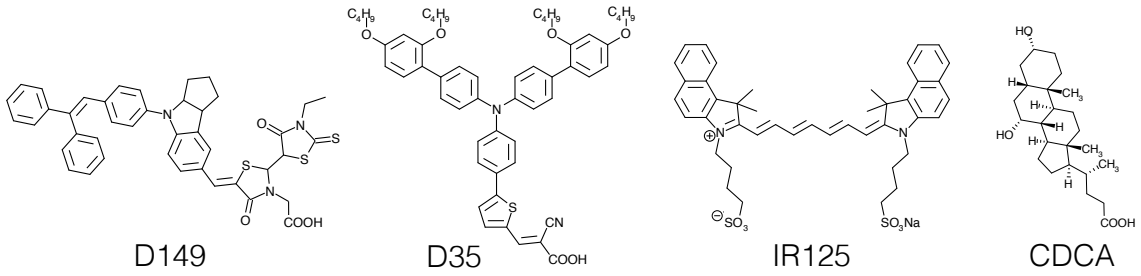

Figure 1: Structures of the D149, D35, and IR125 organic dye sensitizers and the CDCA co-adsorbent.

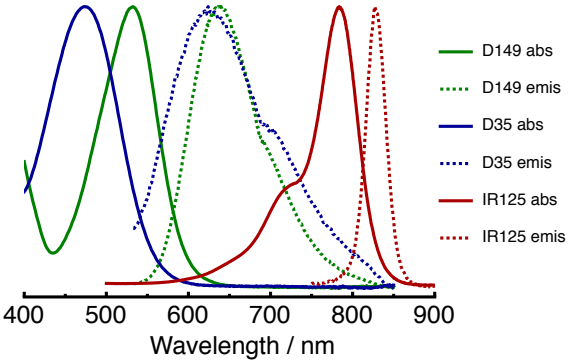

Figure 2: Absorption and emission spectra of the D149, D35, and IR125 organic dye sensitizers in solution.

band and acceptor's absorption band, a short distance between the donor and acceptor (∼1–10 nm), and reasonable alignment between the donor's radiative and acceptor's excitation transition dipole moments. Because the emission bands of D149 and D35 overlap with the absorption band of IR125, the former two dyes should function as FRET donors, with the latter dye acting as a FRET acceptor.

3.2 Spectroscopy of the dye-sensitized zirconia nanoparticles

The dye-sensitized zirconia NPs were deposited on a glass slide and held within a vacuum chamber containing 1 Torr of N_2 buffer gas, where they were probed with laser radiation. This serves our goal of investigating the intrinsic photophysical properties of the dye-sensitized NPs without the complicating influence of solvent or atmospheric contaminants. The ensuing information should serve as a benchmark for computational investigations

of DSSC model systems,[33,34] enabling the theoretical method to be calibrated against well-defined, simple systems.

The investigated dye-sensitized NPs have either a single dye attached (D149, D35, or IR125), or a donor-acceptor combination (D149+IR125 or D35+IR125). Several steps are taken to ensure that the decay of a donor dye's excited state is only due to relaxation back to the ground state (via fluorescence and internal conversion) or FRET, allowing the presence of the latter process to be identified. First, the dyes are attached to zirconia (ZrO_2) NPs, rather than titania (TiO_2), as zirconia's high conduction band-edge prohibits electron injection. Second, to prevent dye aggregation, the dye solutions used to sensitize the NPs contain an excess of the inert chenodeoxycholic acid (CDCA) co-adsorbent (CDCA:donor dye ratio = 50:1), which also binds to the metal-oxide surface.[35–37] This is important as dye aggregates usually relax to the ground state more rapidly than the dye monomer.[36–39] Within co-sensitized systems there is the possibility that the acceptor dye acts as an anti-aggregation agent for the donor dye;[9,15] in our experiment prior removal of the donor dye aggregates ensures that the donor's relaxation rate by fluorescence and internal conversion remains constant between the donor and donor-acceptor cases.

Emission spectra of the dye-sensitized NPs are shown in Figure 3. Excitation of D149-Zr and D35-Zr at 532 nm yields emission bands that have similar profiles and maxima (635 and 625 nm, respectively). Excitation of IR125-Zr at 532 nm did not yield a detectable emission band, unsurprising considering there are no absorption features at this wavelength (Figure 2). The emission spectra are similar to those previously reported for the D149 and D35 dyes attached to zirconia films.[40,41]

Excitation of donor-acceptor NPs (D149+IR125-Zr-C1 and D35+IR125-Zr-C1) at 532 nm produce emission spectra that are composites of the individual dyes' emission bands. The IR125 dye's contribution to the emission is now evident as a new band (maximum at 830 nm) that is not present in the individual D149-Zr and D35-Zr emission spectra. Radiative energy transfer from the excited D149/D35 dye to the IR125 dye will undoubtedly

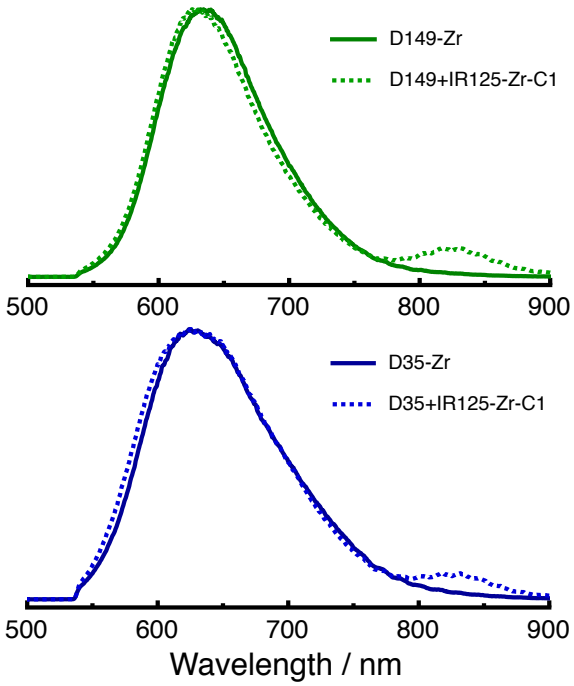

Figure 3: Emission spectra of the D149-Zr and D149+IR125-Zr-C1 samples (top) and D35-Zr and D35+IR125-Zr-C1 samples (bottom).

cause IR125 emission to appear, yet there may also be contributions from FRET.

To examine whether FRET occurs in the co-sensitized samples, we recorded time-resolved fluorescence decays for the donor dyes (D149/D35) after excitation at 532 nm, with and without the acceptor dye (IR125). The lifetime of the excited donor dye in the co-sensitized samples (τ_{D+A}) is determined by the intrinsic relaxation lifetime of the donor dye (τ_D), via fluorescence and internal conversion, and the rate of FRET from the donor dye to the acceptor dye (k_{FRET}):

$$\frac{1}{\tau_{D+A}} = \frac{1}{\tau_D} + k_{FRET} \tag{1}$$

Therefore, if FRET occurs, the donor dye's excited state lifetime will become shorter upon adding the acceptor dye .

Previous studies have found that the fluorescence decays of dye sensitizers on metal-oxide surfaces are non-exponential due to the disordered nature of the dye/surface in-

terface (e.g., surface inhomogeneities, different dye binding modes).[42] To analyse the time-resolved data, we fitted the excited state decay curves to a stretched exponential function [convoluted with the instrument response function (IRF)]:

$$I(t) = I_0 e^{-(\frac{t}{\tau_c})^{\beta}} \tag{2}$$

where I_0 is the initial intensity, τ_c is the characteristic lifetime, and β is the dispersion parameter. The stretched exponential function has been used to model the excited state decays of dye-sensitized surfaces,[39,42,43] with the underlying distribution of first-order decays captured by the β parameter, which has values < 1. Fitted parameters are then used to determine the average lifetime, τ:

$$\tau = \frac{\tau_c}{\beta} \Gamma\left(\frac{1}{\beta}\right) \tag{3}$$

$$\Gamma\left(\frac{1}{\beta}\right) = \int_0^{\infty} x^{\frac{1}{\beta}-1} e^{-x} \mathrm{d}x \tag{4}$$

The donor excited state decay curves recorded for the D149-Zr, D149+IR125-Zr, D35-Zr, and D35+IR125-Zr samples are shown in Figure 4. Fitted and derived parameters from analysis of the decays are given in Table 1.

The τ_D values for D149-Zr and D35-Zr are 1.56 and 1.25 ns, respectively. Fitting the D149-Zr curve to a biexponential function yields lifetimes (44% $\tau_1 = 0.72$ ns, 56% $\tau_2 = 2.51$ ns) that are similar to those measured by El-Zohry *et al.* for the D149 dye on a zironia film using a CDCA:dye = 80:1 sensitizing solution (50% $\tau_1 = 0.70$ ns, 50% $\tau_2 = 2.30$ ns).[40] Lifetimes for the D149 and D35 dyes on a zirconia surface are significantly longer than those measured for the dyes in solution ($\tau \sim 0.2 - 0.3$ ns),[40,41,44–46] with this effect observed previously for organic dye sensitizers, such as D149, and attributed to suppression of excited state isomerization on the surface.[40,47,48]

The τ_{D+A} of the co-sensitized D149+IR125-Zr-C1 sample (1.27 ns) is shorter than that

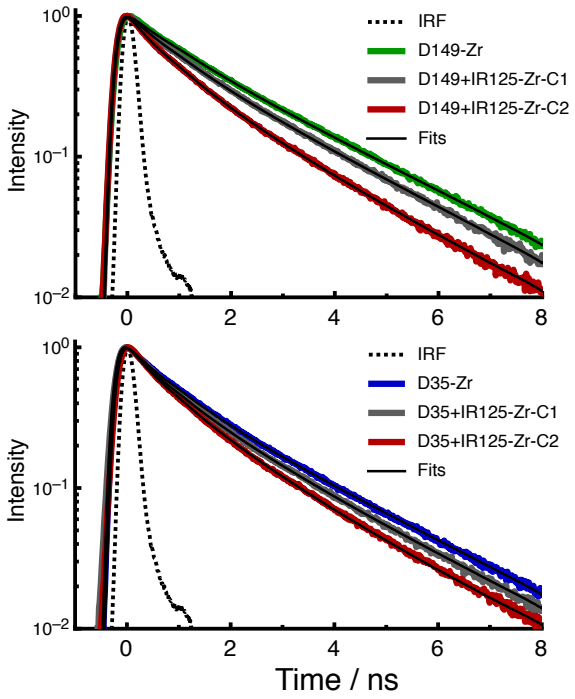

Figure 4: Time-resolved fluorescence decay curves for the D149-Zr and D149+IR125-Zr samples (top) and D35-Zr and D35+IR125-Zr samples (bottom).

of the mono-sensitized D149-Zr sample (1.56 ns), demonstrating that FRET occurs between D149 and IR125 on the zirconia surface. To examine the dependance of FRET on the acceptor dye concentration, we also investigated the D149+IR125-Zr-C2 sample. The increased number of surrounding acceptor dyes per donor dye leads to D149+IR125-Zr-C2 having a shorter τ_{D+A} of 0.89 ns. Using Eq. (1) and the measured lifetimes (τ_D, τ_{D+A}), we estimate k_{FRET} for the D149+IR125-Zr-C1 and D149+IR125-Zr-C2 samples to be 0.15 and 0.48 ns^{-1}, respectively. Alternatively, τ_{D+A} of the co-sensitized D35+IR125-Zr-C1 and D35+IR125-Zr-C2 samples (1.11 and 0.91 ns, respectively) are only slightly shorter than that of the mono-sensitized D35-Zr sample (1.25 ns). This leads to k_{FRET} estimates of 0.10 and 0.30 ns^{-1} for D35+IR125-Zr-C1 and D35+IR125-Zr-C2, respectively, revealing that although FRET also occurs between the zirconia-bound D35 and IR125, it is slower than for the D149+IR125 combination.

From the excited state lifetimes, we can also determine the FRET quantum yield (Φ_{FRET}), which is defined as:

$$\Phi_{FRET} = 1 - \frac{\tau_{D+A}}{\tau_D} \tag{5}$$

The Φ_{FRET} values for D149+IR125-Zr-C1 and D149+IR125-Zr-C2 are 0.19 and 0.43, respectively, whereas for D35+IR125-Zr-C1 and D35+IR125-Zr-C2, the Φ_{FRET} values are 0.11 and 0.27, respectively.

Table 1: Photophysical parameters for the D149-Zr, D149+IR125-Zr, D35-Zr, and D35+IR125-Zr samples derived from the time-resolved fluorescence decay curves.

	β	τ_c/ns	τ_D/ns[a]	τ_{D+A}/ns[b]	k_{FRET}/ns^{-1}	Φ_{FRET}
D149-Zr	0.69	1.21	1.56	-	-	-
D149+IR125-Zr-C1	0.65	0.93	-	1.27	0.15	0.19
D149+IR125-Zr-C2	0.60	0.59	-	0.89	0.48	0.43
D35-Zr	0.68	0.96	1.25	-	-	-
D35+IR125-Zr-C1	0.66	0.83	-	1.11	0.10	0.11
D35+IR125-Zr-C2	0.63	0.64	-	0.91	0.30	0.27

a estimated error ± 0.02 ns
b estimated error ± 0.04 ns

3.3 Experimental Förster distance

From the results described above, it is clear that FRET is less efficient for the D35+IR125 combination than for the D149+IR125 combination. Although k_{FRET} and Φ_{FRET} are sensitive to the donor-acceptor separation distance, the excess of CDCA co-adsorbent used should result in similar donor-acceptor concentrations for D149+IR125 and D35+IR125. To investigate this further we compared the absorption spectra of the sensitizing solutions before and after reaction with the NPs, finding that approximately equal amounts of the D149 and D35 donor dyes are attached to the NPs (D149 $\sim$ 80% adsorbed, D35 $\sim$ 90% adsorbed). Assuming that all the zirconia NPs are 25 nm in diameter, estimated surface coverages for D149-Zr and D35-Zr are 7.97×10^{-2} and 8.97×10^{-2} molecules nm^{-2}, respectively. For IR125, essentially all of the dye is adsorbed, leading to surface coverage estimates of 0.57×10^{-2} and 1.14×10^{-2} molecules nm^{-2} for the donor+IR125-Zr-C1 and donor+IR125-

Zr-C2 samples, respectively. We are unable to estimate the amount of CDCA adsorbed (no strong electronic absorptions in the 200–400 nm UV region were detected), yet we suspect that it is present on the surface in excess compared to the donor dye. This is because in reported studies where CDCA was not used, D35 had around double the surface coverage of D149, due to D35 being able to pack more closely together as it sits perpendicular to the surface, whereas D149 lies almost parallel to the surface.[34,49,50] Therefore, the difference in the FRET rates observed experimentally is believed not to be linked to a donor-acceptor distance effect due to different donor and acceptor dye surface concentrations, but rather results from more efficient FRET coupling for D149+IR125.

The FRET efficiency can be quantified by the Förster distance (R_0), which is the donor-acceptor separation at which the FRET quantum yield is 0.50. To estimate R_0 for the co-sensitized NPs we applied a simple model that assumes the dyes are attached to a flat surface. Although this model does not account for surface curvature of the zirconia NPs and inter-NP FRET, it should be valid because FRET only occurs between neighbouring donor and acceptor dyes molecules which can be considered to lie on a locally flat surface. Wolber and Hudson developed a model for describing FRET between randomly distributed donor and acceptor dyes on a surface, through which R_0 can be derived from the FRET quantum yield and acceptor IR125 dye concentration (see S2).[51,52] By fitting the data for the co-sensitized samples (Figure 5), we arrive at R_0 values of 3.5 and 2.6 nm for the D149+IR125 and D35+IR125 combinations, respectively.

3.4 Theoretical Förster distance

The R_0 of a donor-acceptor pair depends on the donor dye's fluorescence quantum yield (Φ_D), the degree of overlap between the donor's emission and acceptor's absorption spectra, i.e., overlap integral (J), and the relative alignment of the donor and acceptor's transition dipole moments, i.e., orientation factor (κ^2):[32]

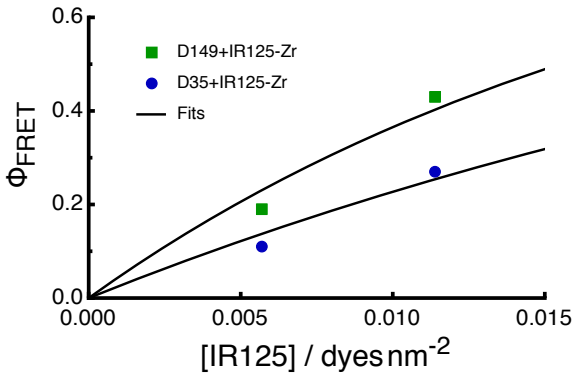

Figure 5: Plot showing the FRET quantum yield against IR125 acceptor dye concentration for the D149+IR125-Zr and D35+IR125-Zr samples. The fits to Eq. S2 (supplementary information) are shown and are used to determine the Förster distances.

$$R_0 = 0.0211 \times (n^{-4} \Phi_D J \kappa^2)^{1/6} \tag{6}$$

where n is the refractive index of the host medium and is taken as 1.68 for our study (see S2).

Unfortunately, these photophysical parameters (Φ_D, J, κ^2) are not available or readily measurable for the dyes attached to zirconia NPs isolated in a vacuum. Nethertheless, we can estimate these parameters using the D149-Zr/D35-Zr emission spectra and τ_D values, the solution-phase spectra, and TD-DFT calculations.

TD-DFT calculations were used to locate the lowest energy isomers of the gas-phase D149, D35, IR125 dyes and predict their electronic absorptions. The CAM-B3LYP functional was used as it is designed to properly describe charge-transfer excitations, although it has been found to overestimate the transition energies.[53] The predicted vertical and adiabatic excitation wavelengths, fluorescence wavelengths, and associated oscillator strengths (given in Table 2) capture the general experimental trends. Although the structures and properties of the isolated dyes will change moderately upon binding to the metal-oxide surface, the results should still provide a guide towards appropriate FRET parameters.

An estimate of Φ_D can be made using the experimental τ_D values, the D149-Zr/D35-Zr fluorescence band maxima, and the TD-DFT oscillator strengths calculated for the $S_0 \leftarrow S_1$

Table 2: TD-DFT spectroscopic parameters for the $S_1 \leftarrow S_0$ transitions of the D149, D35, and IR125 organic dye sensitizers.

	$\lambda_v{}^a$ (nm)	$\lambda_{ad}{}^b$ (nm)	$\lambda_{fl}{}^c$ (nm)	$f_v{}^d$	$f_{fl}{}^e$
D149	418	439	461	1.82	1.92
D35	415	452	485	1.21	1.27
IR125	563	-	-	2.60	-

a vertical excitation wavelength
b adiabatic excitation wavelength
c fluorescence wavelength
d vertical excitation oscillator strength
e fluorescence oscillator strength

transitions of the isolated D149 and D35 dyes. Using these parameters (see S3), we arrive at Φ_D of 0.76 for D149-Zr, compared to 0.41 for D35-Zr.

As seen from Figure 3, the emission bands of D149-Zr and D35-Zr are very similar in both position and profile, suggesting there should be little difference between the donor-acceptor J values. Calculating a value of J appropriate for our experiment requires the absorption spectrum of IR125-Zr in a vacuum, which at this stage is not feasible. Instead, we estimate J using the solution-phase IR125 absorption spectrum (see S4), which should be a reasonable representation of the zirconia-bound spectrum when dye aggregation is prevented with CDCA. For D149+IR125 and D35+IR125, J is estimated to be 4.76×10^{15} and $5.58\times10^{15}\,\mathrm{M^{-1}cm^{-1}nm^4}$, respectively.

The last parameter required to determine R_0 is κ^2. Because the dyes bind to the metal-oxide surface through their acidic group(s), their orientation with respect to the surface is restricted. Consequently, only certain relative donor-acceptor transition dipole moment alignments are possible, limiting the range of κ^2 values.

For D149, which has a rhodanine acetic acid binding motif, surface coverage studies have concluded that the dye lies almost flat along the metal-oxide surface, with DFT simulations supporting this result.[34,49] Similar experimental and theoretical procedures examining triphenylamine-based dyes with cyanoacrylic acid binding motifs, including

D35, have found that they sit almost perpendicular to the metal-oxide surface.[34,50,54,55] In both dyes the carboxylic acid group is predicted to pass its proton to a nearby surface oxygen and then bind to the metal atoms as a carboxylate anion in a bidentate bridging fashion.[34] No information is available on the orientation of IR125 on metal-oxide surfaces, but it is expected that both its sulfonate groups, which bind more strongly to titania than carboxylate groups,[56] will be attached, causing the dye to lie flat along the surface.

TD-DFT calculations allow us to investigate the relative alignment of the transition dipole moments for the D149+IR125 and D35+IR125 pairs. To approximate the dye geometries on the zirconia surface, we have taken the calculated excited state structures of the isolated D149 and D35 dyes and assumed that the two oxygen atoms of the carboxylic acid group bind to the surface, such that the plane defined by the carboxyl oxygen and carbon atoms is perpendicular to the surface. Similarly, the ground state structure of IR125 is assumed to have an oxygen atom from each sulfonic acid group bound to the surface, such that the plane defined by the two SO_3H-C_α bonds is perpendicular to the surface. As shown in Figure 6, D149 and IR125 lie flat along the the surface, whereas D35 is upright with respect to the surface. By analysing the TD-DFT $S_0 \leftarrow S_1$ transitions for the D149 and D35 donor dyes and the TD-DFT $S_1 \leftarrow S_0$ transition for the IR125 acceptor dye, we can calculate the angle (labelled θ) the dye's transition dipole moment is tilted from the axis perpendicular to the surface (Figure 6). For D149, D35, and IR125, we find $\theta = 69^\circ$, 2°, and 90°, respectively. We have also considered a low energy isomer of D35 (D35-i2: $\Delta E = +0.005$ eV), which should also be present on the surface and has $\theta = 35^\circ$. Because the aromatic π system of D149 lies parallel to the surface, low energy cis/trans isomers for D149 should not greatly affect θ.

Although the particular binding motif used by the dye to attach to the surface constrains the angle θ, the dye molecules will have a range of azimuthal angles (ϕ). In Figure 7 we have plotted κ^2 as a function of ϕ_D and ϕ_A for the D149+IR125 and D35+IR125 donor-acceptor pairs. The κ^2 plots clearly show that the D149+IR125 pair sample substantially

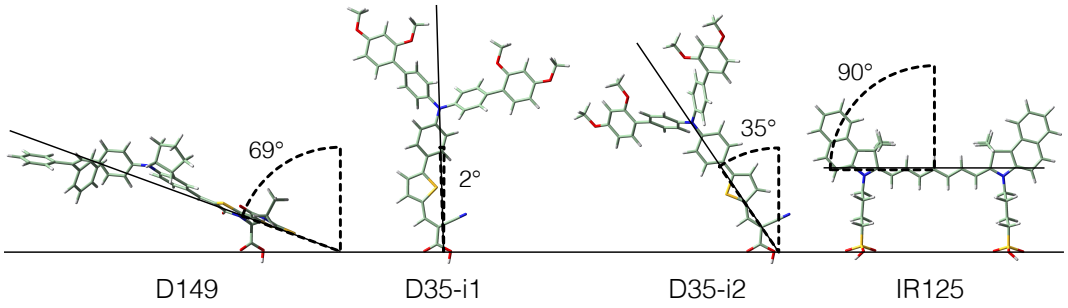

Figure 6: TD-DFT structures for the excited S_1 states of the D149 and D35 (isomers i1 and i2) dyes, and the ground S_0 state of IR125 dye. The angle (θ) of the emission (absorption) transition dipole moment from the axis perpendicular to the surface is given for the D149 and D35 (IR125) dyes.

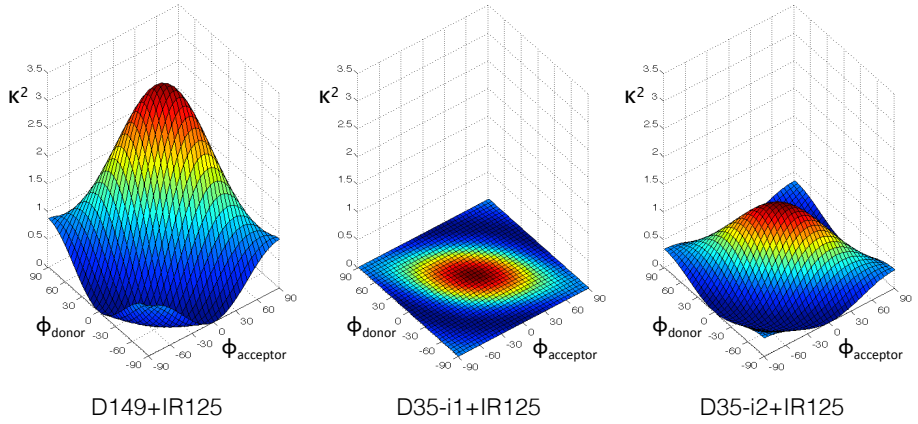

Figure 7: Plots of the orientation factor (κ^2) versus the azimuthal angles of the donor and acceptor (ϕ_D, ϕ_A) for the D149+IR125 (left), D35-i1+IR125 (middle), D35-i2+IR125 (right) donor-acceptor pairs. The θ angles are fixed to those shown in Figure 6.

higher κ^2 values than the D35+IR125 pair. Assuming a random orientation for the two transition dipoles with ϕ_D and ϕ_A ranging from 0 to π, one can calculate an average value for κ^2, which for the D149+IR125 pair is 1.02, whereas for the D35-i1+IR125 and D35-i2+IR125 pairs it is 0.00 and 0.24, respectively. If we assume equal populations of D35-i1 and D35-i2, the average κ^2 value for D35+IR125 is 0.12. The substantial difference in κ^2 values for the D149+IR125 and D35+IR125 pairs arises because the transition dipole moments of D149 and IR125 sample almost collinear arrangements, where κ^2 achieves a maximum value of 4, whereas the transition dipole moments of D35 and IR125 are almost orthogonal, where κ^2 has its minimum value of 0.

Employing the estimated values for Φ_D, J, and κ^2, we arrive at $R_0 = 5.9$ and 3.8 nm for D149+IR125 and D35+IR125, respectively. These distances are somewhat larger than the values estimated from the dependence of Φ_{FRET} on acceptor dye concentration (3.5 and 2.6 nm, respectively), suggesting more efficient FRET, but follow the trend of R_0 being larger for D149+IR125. Again, it is important to emphasise that there are significant assumptions associated with our FRET model: e.g., no other low-lying cis/trans or monodentate binding isomers, well defined surface attachment geometries (i.e., no out-of-plane tilting), and no movement of the dyes.[57] Because J for the two systems is very similar, we can discount this parameter playing a role in the observed variations. On the other hand, both Φ_D and κ^2 favour a longer R_0 for the D149+IR125 pair. Once the dependencies in Eq. (6) are accounted for (e.g., $R_0 \propto (\Phi_D)^{1/6}$, $R_0 \propto (\kappa^2)^{1/6}$), we find that our theoretically determined Φ_D and κ^2 contribute to a 11% and 43% increase, respectively, in R_0 for D149+IR125, relative to D35+IR125. This points to κ^2 being the main source of the experimental R_0 variations determined for the D149+IR125-Zr and D35+IR125-Zr samples.

In summary, our analysis based on estimated FRET parameters supports the longer R_0 derived experimentally for D149+IR125-Zr, relative to D35+IR125-Zr. We contend that this difference is primarily caused by the type of chemical binding groups that attach the dyes to the zirconia surface, which restricts their geometries, creating a more favourable alignment of the transition dipole moments for the D149+IR125 combination.

3.5 Implications for co-sensitized DSSCs

For a DSSC co-sensitized with organic dyes, the occurrence of FRET is considered undesirable, because optical absorbing dyes normally have much higher electron injection efficiencies than near-IR absorbing dyes.[7] This is due to the difficulties in synthesising near-IR organic dye sensitizers that have directional charge-transfer excitations, appropriate molecular orbital energies to drive electron injection and regeneration, long excited state lifetimes, and that do not tend to form dye aggregates. This appears to be the case

for the dyes used in this study, with D149- and D35-based DSSCs achieving incident photon-to-charge carrier efficiencies (IPCEs) in the 70-80% range, whereas IR125-based DSSCs have much lower IPCEs in the ∼2% range.[28–30] The low injection efficiency of IR125 is most likely due to the saturated butyl chains of the binding groups, which restricts the electronic coupling between the dye's π^* excited state and the titania conduction band, and its short excited state lifetime,[30,47] which limits the time available to inject electrons.

Because an excess of CDCA co-adsorbent is used in our study to inhibit dye aggregation, the dye concentrations (D149 and D35: ∼0.09, IR125: ∼0.01 molecules nm^{-2}) are significantly lower than those used in DSSCs, where the dyes are often present at full surface coverage (e.g., D149: ∼0.36, D35: ∼1.47 molecules nm^{-2}).[49,50] However, performing our studies at these higher dye concentrations is not conducive towards obtaining FRET parameters for an equitable comparison of the D149+IR125 and D35+IR125 systems. As mentioned previously, the presence of donor dye aggregates at high coverages would complicate the analysis, as addition of the acceptor dye may act as an anti-aggregation agent,[9,15] which would influence the lifetimes in addition to FRET. Furthermore, within a donor monomer/J-aggregate mixture, excited monomer to aggregate FRET may also occur, followed by aggregate to acceptor dye FRET. In this situation the excitation energy can travel from its original position before FRET to the acceptor, making the model of Wolber and Hudson used to estimate R_0 no longer valid.[51]

Despite the co-sensitized dye-zirconia NP interface being a complex, heterogeneous environment, we have demonstrated that FRET is suppressed in the D35+IR125 system, relative to the D149+IR125 system. In co-sensitized DSSCs, the concentrations of the optical and near-IR dyes are usually adjusted so that the absorption coefficient is reasonably constant across the wavelength absorption range. To consider how the FRET parameters might evolve within functioning DSSCs, we assume a donor dye concentration of 0.36 molecules nm^{-2}, ∼4 times greater than used in our experiments. The Φ_{FRET} is independent of the donor dye concentration, provided only a small fraction is excited at any one

time compared to the acceptor dye concentration,[51] which should be true for typical solar exposure. Because the absorption extinction coefficient of IR125 is ∼5 times that of D35, we assume an acceptor dye concentration of 0.07 molecules nm^{-2}. Under these conditions, if no donor or acceptor dye aggregates are formed, we can predict k_{FRET} and Φ_{FRET} from the fits used to estimate R_0 in Figure 5. We arrive at $k_{FRET} = 8.5$ and 3.2 ns^{-1} and $\Phi_{FRET} = 0.93$ and 0.80 for D149+IR125 and D35+IR125, respectively. The parameters indicate donor dye FRET would effectively compete with electron injection on a titania DSSC electrode.[58] Although the Φ_{FRET} values are now more similar than under our experimental conditions, it does imply that with all else being equal, a D35+IR125 based-DSSC should ultimately achieve a higher solar energy conversion efficiency than a D149+IR125-based DSSC. However, it should be noted that the overall conversion efficiency is influenced by other donor dye properties including the absorption coefficient, absorption range, electron injection efficiency, injected electron-dye cation recombination rate, and redox couple-dye cation regeneration rate. Nevertheless, the strategy of selecting dye binding motifs to encourage donor-acceptor orientations that are unfavorable for FRET may help optimize the conversion efficiencies of co-sensitized DSSCs. Furthermore, FRET could be better suppressed by constructing a well-ordered interface, where the dye sensitizers are constrained to a particular orientation on the surface, perhaps through the introduction of steric substituents or additional acidic anchoring groups, or employing dyes that do not have cis/trans bonds, such as recent porphyrin sensitizers.[4,16]

4 Conclusions

We have used time-resolved fluorescence spectroscopy to investigate zirconia NPs co-sensitized with the IR125 acceptor dye and either the D149 or D35 donor dye. FRET is found to occur between the donor and acceptor dyes, with analysis of the donor dyes' excited state decays revealing that FRET is more efficient for the D149+IR125 combination

than the D35+IR125 combination. By analysing the dependence of the FRET quantum yield on the acceptor dye concentration, the Förster distances for D149+IR125 and D35+IR125 are estimated as 3.5 and 2.6 nm, respectively. By using TD-DFT calculations in conjunction with the experimental data, we conclude that the key parameter controlling the variation in the Förster distance between the two systems is the orientation factor, rather than the donor fluorescence quantum yield or overlap integral. This study suggests that the performance of a co-sensitized DSSC could be enhanced by deliberately misaligning the dyes' transition dipole moments to suppress FRET and enhance the overall electron injection efficiency.

Acknowledgement

This research was supported under the Australian Research Council's Discovery Project funding scheme (Project Number DP120100100). V. Dryza acknowledges an Australian Renewable Energy Agency Postdoctoral Fellowship (6-F004) and support from the University of Melbourne's Early Career Researcher Grant Scheme. The picosecond laser was kindly provided by K. P. Ghiggino and T. A. Smith. The computational portion of this research was undertaken with the assistance of resources provided at the NCI National Facility through the National Computational Merit Allocation Scheme supported by the Australian Government.

Supporting Information Available

Additional material regarding the experimental methods, FRET parameter calculations, and TD-DFT dye structures is available. This material is available free of charge via the Internet at `http://pubs.acs.org/`.

References

(1) O'Regan, B.; Grätzel, M. A Low-Cost, High-Efficiency Solar-Cell based on Dye-Sensitized Colloidal TiO_2 Films. *Nature* **1991**, *353*, 737–740.

(2) Hagfeldt, A.; Boschloo, G.; Sun, L.; Kloo, L.; Pettersson, H. Dye-Sensitized Solar Cells. *Chem. Rev.* **2010**, *110*, 6595–6663.

(3) Hardin, B. E.; Snaith, H. J.; McGehee, M. D. The Renaissance of Dye-Sensitized Solar Cells. *Nat. Photon.* **2012**, *6*, 162–169.

(4) Mathew, S.; Yella, A.; Gao, P.; Humphry-Baker, R.; Curchod, B. F.; Ashari-Astani, N.; Tavernelli, I.; Rothlisberger, U.; Nazeeruddin, M. K.; Grätzel, M. Dye-sensitized Solar Cells with 13% Efficiency Achieved through the Molecular Engineering of Porphyrin Sensitizers. *Nat. Chem.* **2014**, *6*, 242–247.

(5) Ooyama, Y.; Harima, Y. Photophysical and Electrochemical Properties, and Molecular Structures of Organic Dyes for Dye-Sensitized Solar Cells. *ChemPhysChem* **2012**, *13*, 4032–4080.

(6) Ehret, A.; Stuhl, L.; Spitler, M. T. Spectral Sensitization of TiO_2 Nanocrystalline Electrodes with Aggregated Cyanine Dyes. *J. Phys. Chem. B* **2001**, *105*, 9960–9965.

(7) Sayama, K.; Tsukagoshi, S.; Mori, T.; Hara, K.; Ohga, Y.; Shinpou, A.; Abe, Y.; Suga, S.; Arakawa, H. Efficient Sensitization of Nanocrystalline TiO_2 Films with Cyanine and Merocyanine Organic Dyes. *Sol. Energ. Mat. Sol. Cells* **2003**, *80*, 47 – 71.

(8) Yum, J.-H.; Jang, S.-R.; Walter, P.; Geiger, T.; Nuesch, F.; Kim, S.; Ko, J.; Grätzel, M.; Nazeeruddin, M. K. Efficient Co-sensitization of Nanocrystalline TiO_2 Films by Organic Sensitizers. *Chem. Commun.* **2007**, 4680–4682.

(9) Ogura, R. Y.; Nakane, S.; Morooka, M.; Orihashi, M.; Suzuki, Y.; Noda, K. High-

performance Dye-sensitized Solar Cell with a Multiple Dye System. *Appl. Phys. Lett.* **2009**, *94*, 073308.

(10) Siegers, C.; Würfel, U.; Zistler, M.; Gores, H.; Hohl-Ebinger, J.; Hinsch, A.; Haag, R. Overcoming Kinetic Limitations of Electron Injection in the Dye Solar Cell via Coadsorption and FRET. *ChemPhysChem* **2008**, *9*, 793–798.

(11) Brown, M. D.; Parkinson, P.; Torres, T.; Miura, H.; Herz, L. M.; Snaith, H. J. Surface Energy Relay Between Cosensitized Molecules in Solid-State Dye-Sensitized Solar Cells. *J. Phys. Chem. C* **2011**, *115*, 23204–23208.

(12) Hardin, B. E.; Sellinger, A.; Moehl, T.; Humphry-Baker, R.; Moser, J.-E.; Wang, P.; Zakeeruddin, S. M.; Grätzel, M.; McGehee, M. D. Energy and Hole Transfer between Dyes Attached to Titania in Cosensitized Dye-Sensitized Solar Cells. *J. Am. Chem. Soc.* **2011**, *133*, 10662–10667.

(13) Griffith, M. J.; Mozer, A. J.; Tsekouras, G.; Dong, Y.; Wagner, P.; Wagner, K.; Wallace, G. G.; Mori, S.; Officer, D. L. Remarkable Synergistic Effects in a Mixed Porphyrin Dye-sensitized TiO_2 film. *Appl. Phys. Lett.* **2011**, *98*, 163502.

(14) Shrestha, M.; Si, L.; Chang, C.-W.; He, H.; Sykes, A.; Lin, C.-Y.; Diau, E. W.-G. Dual Functionality of BODIPY Chromophore in Porphyrin-Sensitized Nanocrystalline Solar Cells. *J. Phys. Chem. C* **2012**, *116*, 10451–10460.

(15) Pang, A.; Xia, L.; Luo, H.; Li, Y.; Wei, M. Highly Efficient Indoline Dyes Co-sensitized Solar Cells Composed of Titania Nanorods. *Electrochim. Acta* **2013**, *94*, 92 – 97.

(16) Yella, A.; Lee, H.-W.; Tsao, H. N.; Yi, C.; Chandiran, A. K.; Nazeeruddin, M. K.; Diau, E. W.-G.; Yeh, C.-Y.; Zakeeruddin, S. M.; Grätzel, M. Porphyrin-Sensitized Solar Cells with Cobalt (II/III)-Based Redox Electrolyte Exceed 12 Percent Efficiency. *Science* **2011**, *334*, 629–634.

(17) Huang, F.; Chen, D.; Cao, L.; Caruso, R. A.; Cheng, Y.-B. Flexible Dye-sensitized Solar Cells containing Multiple Dyes in Discrete Layers. *Energy Environ. Sci.* **2011**, *4*, 2803–2806.

(18) Jeong, N. C.; Son, H.-J.; Prasittichai, C.; Lee, C. Y.; Jensen, R. A.; Farha, O. K.; Hupp, J. T. Effective Panchromatic Sensitization of Electrochemical Solar Cells: Strategy and Organizational Rules for Spatial Separation of Complementary Light Harvesters on High-Area Photoelectrodes. *J. Am. Chem. Soc.* **2012**, *134*, 19820–19827.

(19) Shankar, K.; Feng, X.; Grimes, C. A. Enhanced Harvesting of Red Photons in Nanowire Solar Cells: Evidence of Resonance Energy Transfer. *ACS Nano* **2009**, *3*, 788–794.

(20) Hardin, B. E.; Hoke, E. T.; Armstrong, P. B.; Yum, J.-H.; Comte, P.; Torres, T.; Frechet, J. M. J.; Nazeeruddin, M. K.; Grätzel, M.; McGehee, M. D. Increased Light Harvesting in Dye-sensitized Solar Cells with Energy Relay Dyes. *Nat. Photon.* **2009**, *3*, 406–411.

(21) Siegers, C.; Hohl-Ebinger, J.; Zimmermann, B.; Würfel, U.; Mülhaupt, R.; Hinsch, A.; Haag, R. A Dyadic Sensitizer for Dye Solar Cells with High Energy-Transfer Efficiency in the Device. *ChemPhysChem* **2007**, *8*, 1548–1556.

(22) Ma, D.; Bettis, S. E.; Hanson, K.; Minakova, M.; Alibabaei, L.; Fondrie, W.; Ryan, D. M.; Papoian, G. A.; Meyer, T. J.; Waters, M. L.; Papanikolas, J. M. Interfacial Energy Conversion in Ru(II) Polypyridyl-Derivatized Oligoproline Assemblies on TiO_2. *J. Am. Chem. Soc.* **2013**, *135*, 5250–5253.

(23) Choi, H.; Cho, N.; Paek, S.; Ko, J. Direct Evidence of Förster Resonance Energy Transfer for the Enhanced Photocurrent Generation in Dye-Sensitized Solar Cell. *J. Phys. Chem. C* **2014**, doi:10.1021/jp407475b.

(24) Schütz, R.; Malhotra, S.; Thomas, I.; Strothkämper, C.; Bartelt, A.; Schwarzburg, K.; Hannappel, T.; Fasting, C.; Eichberger, R. Dynamics of a Covalently Conjoined FRET

Dye Ensemble for Electron Injection into ZnO Nanorods. *J. Phys. Chem. C* **2014**, *118*, 9336–9345.

(25) Odobel, F.; Pellegrin, Y.; Warnan, J. Bio-Inspired Artificial Light-Harvesting Antennas for Enhancement of Solar Energy Capture in Dye-Sensitized Solar Cells. *Energy Environ. Sci.* **2013**, *6*, 2041–2052.

(26) M. J. Frisch *et al.*, Gaussian 09 Revision A.1.

(27) Yanai, T.; Tew, D. P.; Handy, N. C. A New Hybrid Exchange–Correlation Functional using the Coulomb-attenuating Method (CAM-B3LYP). *Chem. Phys. Lett.* **2004**, *393*, 51 – 57.

(28) Horiuchi, T.; Miura, H.; Sumioka, K.; Uchida, S. High Efficiency of Dye-Sensitized Solar Cells Based on Metal-Free Indoline Dyes. *J. Am. Chem. Soc.* **2004**, *126*, 12218–12219.

(29) Jiang, X.; Marinado, T.; Gabrielsson, E.; Hagberg, D. P.; Sun, L.; Hagfeldt, A. Structural Modification of Organic Dyes for Efficient Coadsorbent-Free Dye-Sensitized Solar Cells. *J. Phys. Chem. C* **2010**, *114*, 2799–2805.

(30) Takechi, K.; Sudeep, P. K.; Kamat, P. V. Harvesting Infrared Photons with Tricarbocyanine Dye Clusters. *J. Phys. Chem. B* **2006**, *110*, 16169–16173.

(31) Förster, T. 10th Spiers Memorial Lecture. Transfer Mechanisms of Electronic Excitation. *Discuss. Faraday Soc.* **1959**, *27*, 7–17.

(32) van der Meer, B.; Coker, G.; Chen, S.-Y. *Resonance Energy Transfer: Theory and Data*; VCH Publishers: New York, 1994.

(33) Pastore, M.; Angelis, F. D. First-Principles Computational Modeling of Fluorescence Resonance Energy Transfer in Co-Sensitized Dye Solar Cells. *J. Phys. Chem. Lett.* **2012**, *3*, 2146–2153.

(34) Pastore, M.; De Angelis, F. Intermolecular Interactions in Dye-Sensitized Solar Cells: A Computational Modeling Perspective. *J. Phys. Chem. Lett.* **2013**, *4*, 956–974.

(35) Yum, J. H.; Moon, S. J.; Humphry-Baker, R.; Walter, P.; Geiger, T.; Nuesch, F.; Grätzel, M.; Nazeeruddin, M. d. K. Effect of Coadsorbent on the Photovoltaic Performance of Squaraine Sensitized Nanocrystalline Solar Cells. *Nanotechnology* **2008**, *19*, 424005.

(36) Lu, H.-P.; Tsai, C.-Y.; Yen, W.-N.; Hsieh, C.-P.; Lee, C.-W.; Yeh, C.-Y.; Diau, E. W.-G. Control of Dye Aggregation and Electron Injection for Highly Efficient Porphyrin Sensitizers Adsorbed on Semiconductor Films with Varying Ratios of Coadsorbate. *J. Phys. Chem. C* **2009**, *113*, 20990–20997.

(37) Dryza, V.; Nguyen, J. L.; Kwon, T.-H.; Wong, W. W. H.; Holmes, A. B.; Bieske, E. J. Photophysics and Aggregation Effects of a Triphenylamine-based Dye Sensitizer on Metal-oxide Nanoparticles Suspended in an Ion Trap. *Phys. Chem. Chem. Phys.* **2013**, *15*, 20326–20332.

(38) Muenter, A. A.; Brumbaugh, D. V.; Apolito, J.; Horn, L. A.; Spano, F. C.; Mukamel, S. Size Dependence of Excited-state Dynamics for J-aggregates at Silver Bromide Interfaces. *J. Phys. Chem.* **1992**, *96*, 2783–2790.

(39) Dori, M.; Seintis, K.; Stathatos, E.; Tsigaridas, G.; Lin, T. Y.; Lin, J. T.; Fakis, M.; Giannetas, V.; Persephonis, P. Electron Injection Studies in TiO_2 Nanocrystalline Films Sensitized with Fluorene Dyes and Photovoltaic Characterization. The Effect of Co-adsorption of a Bile Acid Derivative. *Chem. Phys. Lett.* **2013**, *563*, 63–69.

(40) El-Zohry, A.; Orthaber, A.; Zietz, B. Isomerization and Aggregation of the Solar Cell Dye D149. *J. Phys. Chem. C* **2012**, *116*, 26144–26153.

(41) Oum, K.; Lohse, P. W.; Klein, J. R.; Flender, O.; Scholz, M.; Hagfeldt, A.; Boschloo, G.; Lenzer, T. Photoinduced Ultrafast Dynamics of the Triphenylamine-based Organic

Sensitizer D35 on TiO_2, ZrO_2 and in Acetonitrile. *Phys. Chem. Chem. Phys.* **2013**, *15*, 3906–3916.

(42) Kelly, C.; Meyer, G. Excited State Processes at Sensitized Nanocrystalline Thin Film Semiconductor Interfaces. *Cord. Chem. Rev.* **2001**, *211*, 295–315.

(43) Listorti, A.; Lopez-Duarte, I.; Victoria Martinez-Diaz, M.; Torres, T.; DosSantos, T.; Barnes, P. R. F.; Durrant, J. R. Zn(II) versus Ru(II) Phthalocyanine-sensitised Solar Cells. A Comparison Between Singlet and Triplet Electron Injectors. *Energy Environ. Sci.* **2010**, *3*, 1573–1579.

(44) Lohse, P. W.; Kuhnt, J.; Druzhinin, S. I.; Scholz, M.; Ekimova, M.; Oekermann, T.; Lenzer, T.; Oum, K. Ultrafast Photoinduced Relaxation Dynamics of the Indoline Dye D149 in Organic Solvents. *Phys. Chem. Chem. Phys.* **2011**, *13*, 19632–19640.

(45) Fakis, M.; Stathatos, E.; Tsigaridas, G.; Giannetas, V.; Persephonis, P. Femtosecond Decay and Electron Transfer Dynamics of the Organic Sensitizer D149 and Photovoltaic Performance in Quasi-Solid-State Dye-Sensitized Solar Cells. *J. Phys. Chem. C* **2011**, *115*, 13429–13437.

(46) Rohwer, E.; Richter, C.; Heming, N.; Strauch, K.; Litwinski, C.; Nyokong, T.; Schlettwein, D.; Schwoerer, H. Ultrafast Photodynamics of the Indoline Dye D149 Adsorbed to Porous ZnO in Dye-Sensitized Solar Cells. *ChemPhysChem* **2013**, *14*, 132–139.

(47) Sudeep, P. K.; Takechi, K.; Kamat, P. V. Harvesting Photons in the Infrared. Electron Injection from Excited Tricarbocyanine Dye (IR-125) into TiO2 and Ag@TiO2 Core-Shell Nanoparticles. *J. Phys. Chem. C* **2007**, *111*, 488–494.

(48) Zietz, B.; Gabrielsson, E.; Johansson, V.; El-Zohry, A. M.; Sun, L.; Kloo, L. Photoisomerization of the Cyanoacrylic Acid Acceptor Group - a Potential Problem for Organic Dyes in Solar Cells. *Phys. Chem. Chem. Phys.* **2014**, *16*, 2251–2255.

(49) Howie, W. H.; Claeyssens, F.; Miura, H.; Peter, L. M. Characterization of Solid-state Dye-sensitized Solar Cells utilizing High Absorption Coefficient Metal-free Organic Dyes. *J. Am. Chem. Soc.* **2008**, *130*, 1367–1375.

(50) Pazoki, M.; Lohse, P. W.; Taghavinia, N.; Hagfeldt, A.; Boschloo, G. The Effect of Dye Coverage on the Performance of Dye-sensitized Solar Cells with a Cobalt-Based Electrolyte. *Phys. Chem. Chem. Phys.* **2014**, *16*, 8503–8508.

(51) Wolber, P.; Hudson, B. An Analytic Solution to the Förster Energy Transfer Problem in Two Dimensions. *Biophys. J.* **1979**, *28*, 197 – 210.

(52) Urquhart, R. S.; Hall, R. A.; Thistlethwaite, P. J.; Grieser, F. Förster Energy Transfer in Two-dimensional Amphiphile Arrays at the Air/Water Interface. *J. Phys. Chem.* **1990**, *94*, 4173–4182.

(53) Dev, P.; Agrawal, S.; English, N. J. Determining the Appropriate Exchange-correlation Functional for Time-dependent Density Functional Theory Studies of Charge-transfer Excitations in Organic Dyes. *J. Chem. Phys.* **2012**, *136*, 224301.

(54) Jiang, X.; Karlsson, K. M.; Gabrielsson, E.; Johansson, E. M. J.; Quintana, M.; Karlsson, M.; Sun, L.; Boschloo, G.; Hagfeldt, A. Highly Efficient Solid-State Dye-Sensitized Solar Cells Based on Triphenylamine Dyes. *Adv. Funct. Mater.* **2011**, *21*, 2944–2952.

(55) Zuleta, M.; Edvinsson, T.; Yu, S.; Ahmadi, S.; Boschloo, G.; Gothelid, M.; Hagfeldt, A. Light-induced Rearrangements of Chemisorbed Dyes on Anatase(101). *Phys. Chem. Chem. Phys.* **2012**, *14*, 10780–10788.

(56) Ambrosio, F.; Martsinovich, N.; Troisi, A. What Is the Best Anchoring Group for a Dye in a Dye-Sensitized Solar Cell? *J. Phys. Chem. Lett.* **2012**, *3*, 1531–1535.

(57) Brennan, T. P.; Tanskanen, J. T.; Bakke, J. R.; Nguyen, W. H.; Nordlund, D.; Toney, M. F.; McGehee, M. D.; Sellinger, A.; Bent, S. F. Dynamical Orientation of Large Molecules

on Oxide Surfaces and its Implications for Dye-Sensitized Solar Cells. *Chem. Mat.* **2013**, *25*, 4354–4363.

(58) Listorti, A.; O'Regan, B.; Durrant, J. R. Electron Transfer Dynamics in Dye-Sensitized Solar Cells. *Chem. Mat.* **2011**, *23*, 3381–3399.

Graphical TOC Entry